Applied Environmental Research
- RESEARCH FOR SUSTAINABLE PLANET -

Research Article

Adsorption Behavior and Mechanism of Brilliant Green Dye onto Acid-modified Mesoporous Volcanic Pumice

Suchada Sawasdee*, Prachart Watcharabundit

Thepsatri Rajabhat University, Department of Chemistry, Lopburi, Thailand

*Correspondence Email: suchada.s@lawasri.tru.ac.th

Abstract

Water pollution is a major problem in the environment. The important one is the dying effluent from the textile industry. Dye effluent has affected human health and aquatic life. Recently, natural adsorbents have been most commonly used for dye treatment wastewater. This study explores the adsorption mechanism of brilliant green onto HCl-modified pumice. It involves a comparative analysis of the raw and HCl-modified pumice's characterization and adsorption properties. The adsorption experiments were carried out by considering several parameters, such as pH, contact time, initial dye concentrations, and temperatures. The research indicated that the raw and acid-treated pumice possess Si-OH and Si-O-Si groups. These pumice adsorbents are classified as mesoporous, exhibiting BJH pore diameters of 3.23 nm for the raw form and 3.69 nm for the acid-modified variant. The adsorption data revealed that the uptake of brilliant green dye was maximal at a pH of 8. The equilibrium results closely matched the Langmuir isotherm model. The maximum adsorption capacities were 37.13, 40.17, and 42.73 mg g^{-1} for the raw pumice, and 46.72, 51.81, and 56.17 mg g^{-1} for the modified pumice at 20, 30, and 40 °C, respectively. Furthermore, the removal efficiency of brilliant green dye with modified pumice was 91.93%, 95.29%, and 96.27% at 20°C, 30°C, and 40°C, respectively. The pseudo-second-order model was the most suitable for elucidating the kinetic adsorption data. The thermodynamic analysis revealed that the adsorption process was endothermic, spontaneous, and physical. Dipole-dipole H-bonding interaction, Yoshida H-bonding, electrostatic interaction, n-π interaction, cation exchange, and pore filling were all engaged in its process. Consequently, the local pumice volcanic rock became a great, cheap, abundant, and environmentally friendly adsorbent for removing dyes from effluents.

ARTICLE HISTORY
Received: 21 Mar. 2024
Accepted: 5 Aug. 2024
Published: 16 Sep. 2024

KEYWORDS
Adsorption;
Isotherm;
Kinetics;
Brilliant green;
Volcanic pumice;
Mechanism

Introduction

All living things need water and access to water resources to have a sufficient amount of food and a healthy environment. The need for freshwater worldwide has been rising quickly as human populations and economies expand. Water contamination occurs due to highly soluble hazardous substances originating from industrial wastes, agrochemical wastes, and domestic sewage. Water resources can include harmful pollutants such as plastics, heavy metal ions, dyes, and medical waste [1]. Dyes are colored compounds that are used primarily for aesthetic and attractiveness purposes. They are currently widely used in a variety of industries, including textiles, printing, paper, food, medicine, and so on. Dyes are divided into two big groups: natural dyes and synthetic dyes. Al-Shehri et al. [2] noted that the annual production of synthetic dyes exceeds 700,000 tons, including around 10,000 different varieties. Approximately 15% of the dye is discharged into the environment as effluent during dyeing, resulting in environmental

https://doi.org/10.35762/AER.2024042

issues [3]. Since dyes frequently show resistance to heat, oxidizing agents, light, and many chemicals, the dye color itself is the main contaminant in dye wastewater [4].

Synthetic dyes are noticeable and evoke displeasure in water, even at a comparatively low concentration of 1 part per million (ppm) [5]. Dyes, a type of organic colorant, reduce the amount of sunlight reaching the water's surface, which negatively impacts aquatic ecosystems by inhibiting photosynthesis. Synthetic dyes may be categorized into three separate groups: cationic dyes, commonly referred to as basic dyes; anionic dyes, which include direct, acidic, and reactive dyes; and non-ionic dyes, notably dispersion dyes [4]. According to El-Sayed et al. [6], cationic dyes have a greater risk in terms of toxicity, mutagenicity, and carcinogenicity compared to anionic dyes. This heightened risk can be attributed to their synthetic nature and possessing an aromatic ring structure with delocalized electrons. Brilliant green (BG), a cationic dye, has been used as a biocide in the coloring industry, but it also has several medical and therapeutic uses, including as an anthelminthic and disinfectant. It is dangerous, and it can even cause cancer. Furthermore, BG promotes tumor formation in mammalian liver cells [7].

Treatment of wastewater before discharge is necessary to guarantee that it meets all applicable standards [8]. To remove dyes from wastewater, several procedures such as biological treatment, coagulation, flotation, electrochemical techniques, adsorption, and oxidation can be applied. Adsorption is a common and effective technique for removing dyes from industrial effluent. Activated carbons are the most commonly utilized adsorbent for dye effluent due to their high adsorption capacity and huge surface area. Despite this, they are rarely employed because of their high cost [9–10]. Recently, researchers have concentrated on adsorbents that are affordable, widely available, effective, and easily accessible, such as industrial waste, agricultural waste, and natural inorganic minerals. One of the most effective adsorbents for the treatment of cationic dyes is natural inorganic materials. Pumice, a volcanic rock, is a natural inorganic material. It is a simple-to-use and inexpensive material whose primary component is aluminum silicate, mostly made of silica (SiO_2) and alumina (Al_2O_3). A material's surface silicon atoms can create silanol, which serves as an adsorption site [11–12].

Natural adsorbents frequently exhibit substantial levels of contaminants and have limited adsorption capacity. The adsorption capabilities of modified adsorbents are enhanced compared to their unmodified counterparts as a result of alterations in the specific surface area, pore structure, and surface functional groups of the adsorbent. To create effective adsorbents, researchers employed heat, acid, and alkaline activation techniques. The efficacy of acid treatment in enhancing the surface area, pore volume, and negative surface charge of kaolin has been demonstrated [13]. Acid-modified surfaces of adsorbents make them more hydrophilic and more acidic by reducing the number of minerals on their surfaces [5]. Olasehinde and Abegunde [14] utilized hydrochloric acid (HCl) as a modifier in producing activated carbon from Raphia taedigera seeds, observing a clustered and irregular structure that enhanced pore formation. Indah et al. [15] determined that HCl demonstrated more effective acidic characteristics than H_2SO_4 and HNO_3 for modifying pumice and extracting Cu(II) from aqueous solutions. Similarly, Silva et al. [16] investigated the removal of cationic and anionic dyes from water using acid-treated Brazilian palygorskite and found that 2 M HCl was a more effective modifying solution than 4 M HCl and 6 M HCl. Researchers have used pumice to remove dyes and metal ions from aqueous solutions [17–21]. This is because pumice is inexpensive and has a high level of porosity. Pumice is an indigenous geological substance that is found in the vicinity of Lopburi, Thailand. Therefore, we are interested in studying the previously unreported process of cationic dye adsorption employing the particular local pumice from Lopburi as an adsorbent. This study analyzed the raw pumice and the HCl-modified pumice to determine their surface area, pore size distribution, structural and chemical properties, as well as functional groups. The study utilized batch adsorption as a tool to examine certain adsorption conditions. In addition, the investigation focused on characterizing the adsorbent and analyzing the adsorption data to determine the fundamental mechanism of BG dye adsorption onto the HCl-modified pumice.

Materials and methods

1) Adsorbate

Figure 1 shows the chemical structure of BG (CI 420140, molecular formula $C_{27}H_{34}N_2SO_4$, molecular weight = 482.65 g mol^{-1}; Merck, Germany) dye. In preparation for the dye solution, the stock solution was prepared at 1,000 mg L^{-1}, then diluted to the required concentrations of the working solution.

The analytical-grade sodium hydroxide (NaOH), HCl, and sodium nitrate ($NaNO_3$) were purchased from Merck & Co.

2) Preparation of adsorbent

The raw natural pumice was obtained from the Sabot District in Lopburi Province, Thailand. To remove any contaminants, the pumice was thoroughly washed

with tap water and then dried in a hot air oven. The dried pumice was classified into two groups: raw and modified. To modify the pumice, we immersed 20 g of the dried, raw pumice in 200 mL of 2.0 M HCl, maintaining the mixture at room temperature and stirring continuously at 100 revolutions per minute (rpm) for 24 hours. Afterward, the acid-treated pumice was neutralized with double-distilled water and oven-dried. Both the raw and modified pumice were then sieved through a 50–100 mesh for further use.

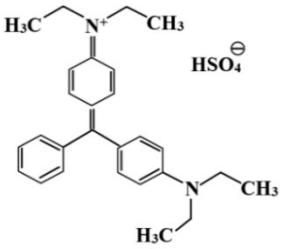

Figure 1 BG dye structure.

3) Characterization of adsorbent

The properties of the raw and modified pumice employed as the adsorbent in this investigation were carefully analyzed. The surface properties of the raw and modified pumice, including their surface area and pore structure, were investigated using N_2 adsorption measurements conducted at a temperature of 77 K using the Autosorb 1 MP instrument and Quantachrome Nova Win software. The structural study was conducted via X-ray diffraction (XRD) with the PANalytical X'Pert Pro MPD model. The chemical compositions of raw and modified pumice were analyzed using X-ray fluorescence spectrometry with the HORIBA MESA-500W model. The external surfaces of both pumices were scrutinized using a scanning electron microscope (SEM), specifically the LEO 1450 VP model. The functional groups of the two pumice were identified through Fourier transform infrared spectroscopy (FTIR) utilizing a Perkin Elmer instrument, Type 2.

4) Batch experimental design

Batch adsorption tests with the raw and modified pumice adsorbents were performed under various conditions, including pH (2, 3, 4, 5, 6, 7, 8, 9, 10) of dye solutions, contact time (5, 10, 15, 30, 45, 60, 90, 120, 150, 180, 210, 240, 300 min), BG solution concentrations (50, 100, 150, 200, 250, 300 mg L^{-1}), and temperatures (20°, 30°, 40 C). BG dye solutions were treated with pH modification using solutions of HCl and NaOH at concentrations of 0.1 M. The experiments were carried out using a controlled-temperature shaker (DAIHAN SCIENTIFIC, KOREA, IS-10R) at 200 rpm, with 100 mL of BG dye solution and 0.5 g of pumice. The suspended particles in each sample were filtered for a specified amount of time, and the amount of BG dye in the filtrate was measured with a double-beam UV-visible spectro-photometer (Analytik Jena, Specord 210 plus, Germany) at 625 nm. The adsorption capacity at any time (q_t) and at equilibrium time (q_e) was determined using Eq. 1 and 2, respectively. Additionally, Eq. 3 was used to calculate the removal efficiency (%).

$$q_t = \frac{(C_o - C_t)V}{W} \quad \text{(Eq. 1)}$$

$$q_e = \frac{(C_o - C_e)V}{W} \quad \text{(Eq. 2)}$$

$$\text{Removal efficiency (\%)} = \frac{(C_o - C_e)}{C_o} \times 100 \quad \text{(Eq. 3)}$$

where C_o (mg L^{-1}) and C_t (mg L^{-1}) are the BG dye concentration at the beginning and at any time, respectively. C_e (mg L^{-1}) is the BG dye concentration at equilibrium time, V (L) is the volume of the solution, and W (g) is the mass of the pumice adsorbent.

5) Adsorption isotherm

Adsorption isotherm tests are conducted under equilibrium and at a constant temperature. The investigation employed the Langmuir, Freundlich, and Dubinin-Radushkevich isotherm equations. The linear expression of the Langmuir isotherm is given by Eq. 4 [1]:

$$\frac{C_e}{q_e} = \frac{1}{q_{max}} C_e + \frac{1}{K_L q_m} \quad \text{(Eq. 4)}$$

where K_L is a constant and q_{max} (mg g^{-1}) is the maximum adsorption capacity of BG dye on the pumice adsorbents.

The Langmuir isotherm can be better understood by considering the parameter R_L, which has been defined as:

$$R_L = \frac{1}{(1+K_L C_o)} \quad \text{(Eq. 5)}$$

The value R_L serves as an indicator of the isotherm's form, which may be classified as unfavorable ($R_L > 1$), linear ($R_L = 1$), favorable ($0 < R_L < 1$), or irreversible ($R_L = 0$).

The Freundlich isotherm in a linear form is represented as follows [1]:

$$\log q_e = \log K_F + 1/n \log C_e \quad \text{(Eq. 6)}$$

where K_F (L g^{-1}) is the Freundlich constant and 1/n is the adsorption intensity or surface heterogeneity. The value of 1/n falls between the range of more than 0 and less than 1 for adsorption which is considered favorable.

The linear representation of the Dubinin-Radushkevich isotherm is given by Eq. 7 [1]:

$$\ln q_e = \ln q_o - K_{DR}\ [RT \ln(1 + 1/C_e)]^2 \qquad \text{(Eq. 7)}$$

where K_{DR} (mol^2 kJ^{-2}) and q_o (mg g^{-1}) are calculated from the slope and intercept of the graph plotted between ln q_e and [RT ln (1+1/C_e)]2. The mean adsorption energy, E (kJ mol^{-1}), is calculated as Eq. 8:

$$E = \frac{1}{\sqrt{2K_{DR}}} \qquad \text{(Eq. 8)}$$

where K_{DR} is the Dubinin-Radushkevich constant. According to Dinh et al. [19, 22], adsorption may be described as a physical phenomenon occurring when the energy (E) of the system is below 8 kJ mol^{-1}. The adsorption process may be classified as ion exchange when the energy (E) falls within the range of 8 to 16 kJ mol^{-1}. Moreover, if the energy exceeds 16 kJ mol^{-1}, it can be classified as chemisorption.

6) Adsorption kinetics

The kinetic adsorption was analyzed for the determination of the rate and mechanism of adsorption. Its experimental data were the adsorption capacity at any time. Eqs. 9 and 10 offer the pseudo-first-order and pseudo-second-order equations, respectively, which are employed in the assessment of the kinetic study.

$$\log (q_e - q_t) = log q_e - \frac{k_1}{2.303} t \qquad \text{(Eq. 9)}$$

$$\frac{t}{q_t} = \frac{1}{k_2 q_e^2} + \frac{1}{q_e} t \qquad \text{(Eq. 10)}$$

The initial rate constant (h) is defined by:

$$h = k_2 q_e^2 \qquad \text{(Eq. 11)}$$

where k_1 and k_2 are the rate constants of the pseudo-first-order and the pseudo-second-order, respectively. Additionally, h (mg g^{-1} min^{-1}) is the initial adsorption rate as t→0.

The mathematical representation of the intraparticle diffusion model may be found in Eq. 12.

$$q_t = K_{id}(t)^{1/2} + C \qquad \text{(Eq. 12)}$$

where K_{id} represents the rate constant of the intraparticle diffusion model, and C denotes the constant about the boundary layer.

7) Thermodynamic of adsorption

The thermodynamic study will evaluate the adsorption capacity under conditions of equilibrium and varying temperatures. The adsorption data at different temperatures were used to study the thermodynamic parameters, such as the change in Gibbs free energy (ΔG), enthalpy (ΔH), and entropy (ΔS). In the context of the adsorption process, the Gibbs free energy change (ΔG) may be expressed in the following manner [23]:

$$\Delta G = -RT \ln K_e \qquad \text{(Eq. 13)}$$

In the above equation, K_e (=q_e/C_e) represents the equilibrium constant, R denotes the gas constant (8.314 J K^{-1} mol^{-1}), and T signifies the absolute temperature in Kelvin (K). Additionally, the determination of changes in enthalpy (ΔH) and entropy (ΔS) may be achieved by the utilization of the subsequent equations:

$$2.303 \log K_e = \frac{\Delta S}{R} - \frac{\Delta H}{RT} \qquad \text{(Eq. 14)}$$

$$\log K_e = \frac{\Delta S}{2.303R} - \frac{\Delta H}{2.303RT} \qquad \text{(Eq. 15)}$$

Results and discussion

1) Characterizations of adsorbent

1.1) Surface area and pore size distribution analysis

The raw and modified pumice were analyzed using a nitrogen adsorption-desorption isotherm. Figure 2 (a and c) presents the isotherms for both materials. In the case of raw pumice, adsorption levels rose with increasing relative pressure (P/P0), whereas the adsorption for modified pumice stayed uniform until a relative pressure of 0.4 was attained. Beyond this point, the adsorption for modified pumice increased progressively with higher relative pressures. The results in Figure 2 (a and c) and the classification set by the International Union of Pure and Applied Chemistry (IUPAC) make it clear that the isotherm had properties that were consistent with type IV, and it also had an H3 hysteresis loop. Sun et al.'s investigation [24] showed that the nitrogen adsorption of CA/Ben followed an IV isotherm with the H3 hysteresis loop, corresponding to the present study's findings. The observed isotherm of type IV indicates that the adsorbent material possesses mesoporous characteristics and is associated with the phenomenon of capillary condensation. The occurrence of the H3-type hysteresis loop may be ascribed to the phenomenon of capillary condensation transpiring inside a texture that lacks rigidity [25]. The determination of surface area was carried out utilizing the Brunauer–Emmett–Teller (BET) methodology, whilst the evaluation of pore size

distribution (Figures 2b and 2d) was accomplished employing the Barret–Joyner–Halenda (BJH) method.

Table 1 shows that the surface area of the raw and modified pumice was 12.020 and 3.739 $m^2 g^{-1}$, respectively. The reduction in BET surface area of the modified pumice may be attributed to the coverage and collapse of pores during acidification [26–27], along with a decrease in microporosity and an increase in mesoporosity [28]. The adsorbents' pore widths may be classified into three distinct categories: micropore, mesopore, and macropore. Micropores are characterized by dimensions that are smaller than 2 nm, whereas mesopores exhibit diameters between the ranges of 2 to 50 nm. Macropores, on the other hand, possess sizes above 50 nm. The pore size distribution study revealed that the pore diameters of raw pumice ranged from 3.05 to 1623.10 nm, whereas those of modified pumice varied from 3.11 to 118.79 nm. Pore diameters ranging from 3 to 50 nm were observed in approximately 91.07% and 82.20% of the pore volume of the raw and modified pumice, respectively. The pore sizes observed in the raw and modified pumice primarily range from about 3 nm to 15 nm, as depicted in Figures 2b and 2d. The findings indicated that the main pore size of the raw and modified pumice was mostly in the mesoporous range. In addition, Table 1 presents the typical characteristics of raw and modified pumice. The BET total pore volume for modified pumice (0.023 $cm^3 g^{-1}$) is greater than that of raw pumice (0.021 $cm^3 g^{-1}$). The pore diameter (Dp, nm) calculation utilized the Wheeler Equation ($Dp = 4000*(Vp / S_{BET})$), following the method referenced by Mansour et al. [29], where Vp ($cm^3 g^{-1}$) is the total pore volume of nitrogen liquid at 0.99 P/P_0 and S_{BET} ($m^2 g^{-1}$) is the specific surface area. The BET pore diameter of the raw pumice was 6.99 nm, whereas the modified pumice had a pore diameter of 24.60 nm. Furthermore, the pore size distribution, determined by the BJH method from the adsorption branch (Figure 2 (b, d)), revealed that the modified pumice possesses a larger pore size of 3.69 nm in contrast to the 3.23 nm pore size of the raw pumice.

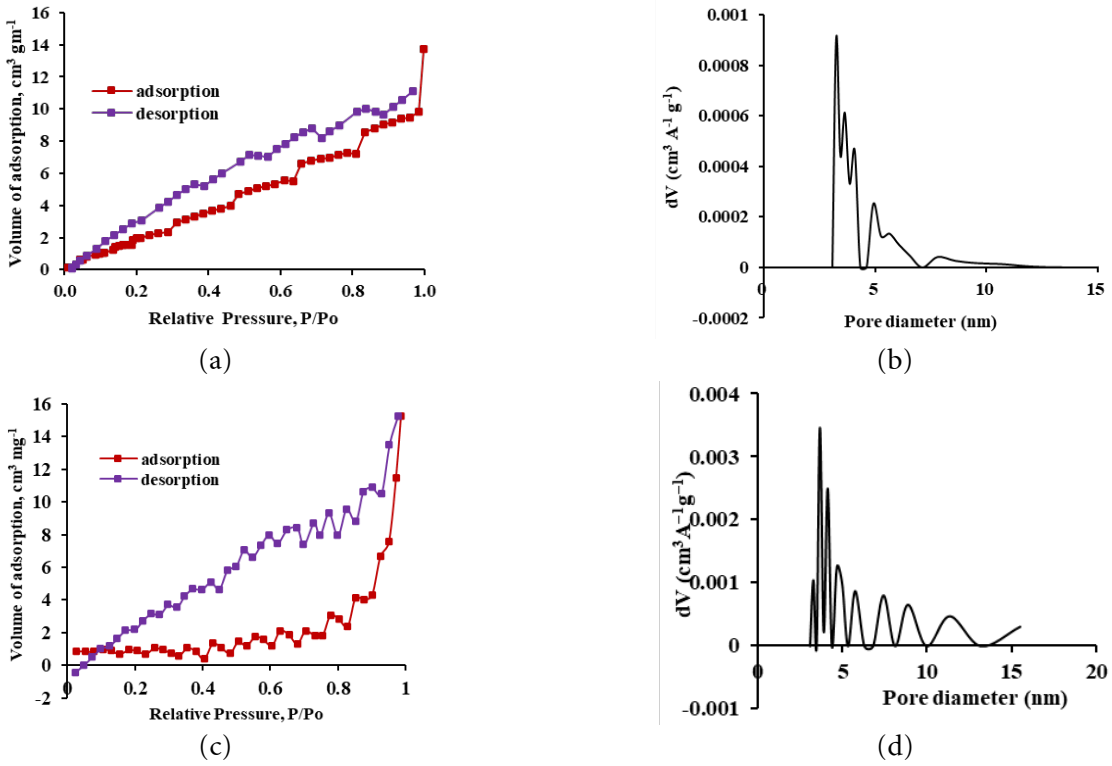

Figure 2 (a) Nitrogen adsorption-desorption isotherm and (b) BJH pore size distribution of the raw pumice (c) nitrogen adsorption-desorption isotherm and (d) BJH pore size distribution of the modified pumice.

Table 1 Characteristic parameters of the raw and modified pumice

Parameters	Adsorbents	
	Raw pumice	Modified pumice
BET surface area ($m^2 g^{-1}$)	12.020	3.739
BET total pore volume ($cm^3 g^{-1}$)	0.021	0.023
BET average pore diameter (nm)	6.99	24.60
BJH desorption median pore diameter (nm)	3.23	3.69

Table 2 The XRF data of the raw and modified pumice before and after adsorption of BG dye

Weight (%)	Adsorbents			
	Raw pumice		Modified pumice	
	Before adsorption	After adsorption	Before adsorption	After adsorption
SiO_2	69.79	69.52	69.96	69.52
K_2O	23.79	23.67	23.83	23.67
Al_2O_3	2.72	2.97	2.70	2.96
Fe_2O_3	2.32	2.23	2.23	2.22
TiO_2	0.65	0.67	0.64	0.63
Rh_2O	0.07	0.65	0.45	0.65
ZrO_2	0.11	0.11	0.08	0.11
Rb_2O	0.44	0.09	0.07	0.08

1.2) XRF analysis

Table 2 shows the chemical compositions of the raw and modified pumice as determined by XRF analysis. As seen in Table 2, the modified pumice contained higher amounts of SiO_2 and K_2O compared to the raw pumice. The main chemical components identified were SiO_2, K_2O, Al_2O_3, and Fe_2O_3. Other elements like TiO_2, Rh_2O, ZrO_2, and Rb_2O were present as trace elements. After adsorption, the proportions of SiO_2, K_2O, and Fe_2O_3 were reduced in both raw and modified pumice, suggesting their participation in the ion exchange process with the dye molecules [30].

1.3) XRD analysis

The XRD pattern of the raw and modified pumice, as depicted in Figure 3 (a and b), exhibits a significant rise in the background line within the range of $2\theta = 20°$ to 30°. This observation confirms the existence of amorphous silica within the pumice sample [1, 31]. The raw pumice sample displayed peaks at 2θ angles of 21.9°, 23.7°, 27.7°, 28.0°, 31.3°, 35.5°, 42.1°, 45.5°, 49.7°, 53.4°, 55.2°, 61.8°, and 62.3°. The modified pumice sample revealed peaks at 2θ angles of 21.9°, 22.8°, 23.6°, 23.7°, 24.3°, 24.5°, 26.3°, 27.7°, 28.0°, 28.3°, 29.6°, 30.3°, 30.5°, 31.4°, 35.7°, 36.7°, 42.1°, 50.6°, 53.1°, 54.2°, 55.3°, 58.2°, 60.7°, 62.0°, 64.8°, 66.2°, 67.7°, 69.5°, 73.4°, and 78.0°. The peaks observed at 2θ angles indicate the presence of crystalline phases. The average size of the crystalline phases, estimated using the Scherrer equation, was approximately 77.09 nm for raw pumice and 91.4 nm for modified pumice.

1.4) SEM analysis

The external appearance of the raw and modified pumice was analyzed with a SEM method. Empirical evidence supporting the heterogeneous nature of the adsorbents is provided by observation of many irregular pores on the surface of the raw and modified pumice, as seen in Figure 4 (a and b). The adsorbent material exhibited notable characteristics, including a significant surface roughness and porosity, along with a multitude of holes of varying sizes dispersed throughout its structure. Additionally, the SEM image revealed that the modified pumice was cleaner than the raw pumice. The modified pumice featured pores with expanded cavities, while the raw pumice exhibited shallow pores and signs of cracking.

1.5) The point of zero charge (pH_{pzc}) of the raw and modified pumice

The determination of the pH at the point of zero charges (pH_{pzc}), which refers to the pH value at which the surface charge of a material is neutral, was conducted using the pH drift technique [32]. During the tests, a quantity of 0.1 g of raw pumice and modified pumice were introduced into a sequence of 100 mL solutions containing 0.1 M $NaNO_3$ with an adjusted pH ranging from 2 to 10. The pH of the solution was modified by the addition of 0.1 M HCl and 0.1 M NaOH, and its pH was determined using an Ohaus pH meter from the United States. The resulting mixtures were subjected to agitation at a speed of 150 rpm for 48 hours. The filtration process was performed on each mixture, followed by measuring its pH (final pH). The pH_{pzc} was determined by identifying the point where the curve, formed by plotting the final pH against the initial pH, intersects with the line representing the situation where the final pH is equal to the initial pH. As indicated in Figure 5 (a and b), the values for the raw and acid-modified pumice are approximately 6.3 and 5.7, respectively. Consequently, acid modification of pumice can enhance its surface acidity.

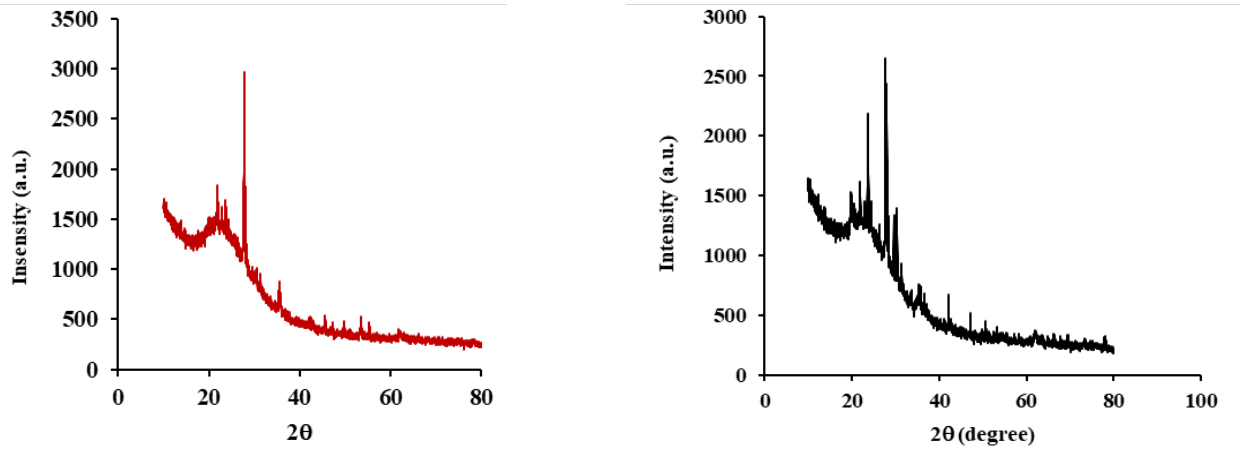

(a) (b)

Figure 3 XRD spectrum of the (a) raw and (b) modified pumice adsorbents.

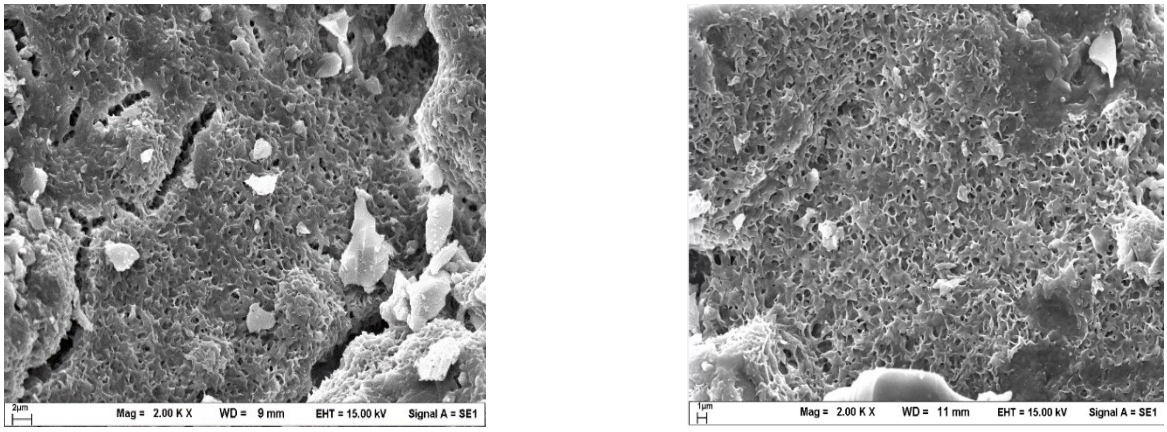

(a) (b)

Figure 4 SEM of the (a) raw and (b) modified pumice adsorbents.

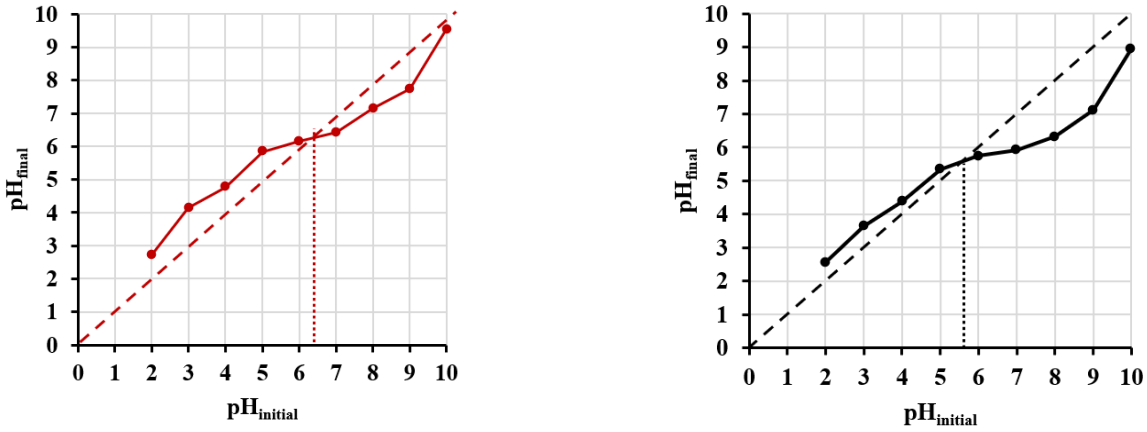

(a) (b)

Figure 5 pH_{pzc} determination of the (a) raw and (b) modified pumice.

1.6) FTIR spectra analysis

Figure 6 (a and b) exhibits the FTIR spectra of the raw and modified pumice before and after dye adsorption throughout the wavelength range of 500 cm^{-1} to 4000 cm^{-1}. The spectra show sharp band vibrations between 500 and 1300 cm^{-1}. The wavenumber of the raw pumice has altered in the modified pumice, showing shifts from 3,620 to 3,673 cm^{-1}, 1,626 to 1,651 cm^{-1}, 1,000 to 1,043 cm^{-1}, and 791 to 782 cm^{-1}. These changes in wavenumber could be attributed to acid activation. The absorption band at 3,620 cm^{-1} in the spectra of the raw pumice and at 3,673 cm^{-1} in the spectra of the modified pumice is attributed to OH stretching vibrations [33]. At this point, the peak was due to free silanol groups (Si-OH) on the surface of the adsorbent [34]. The peak at 1,626 and 1,651 cm^{-1} corresponded to the stretching

vibration of O-H [35]. Siloxane (Si-O-Si) stretching vibrations in and out of the plane were seen as strong bands between 820 cm^{-1} and 1,300 cm^{-1}, specifically at 820 and 1,000 cm^{-1} and 1,043 cm^{-1} [12]. The band at 791 cm^{-1} in the spectra of the raw pumice and 782 cm^{-1} in the spectra of the modified pumice corresponded to the bending vibrations of Si-O-Si, as reported by Sepehr et al. [36]. Ersoy et al. [31] suggested that the peaks observed around 800 cm^{-1} may be attributed to the bending of the Si-O bonds in the amorphous quartz. Therefore, the predominant functional groups of the raw pumice and modified pumice are Si-O-Si and Si-OH.

Adsorption on the raw pumice (Figure 6a) diminished the absorption strength relative to the initial state. Furthermore, a shift in the wavenumber from 791 to 820 cm^{-1} was noted, without significant changes in the other wavenumbers. After being adsorbed onto the modified pumice (Figure 6b), the study revealed that the main bands in the spectra of the dye-saturated adsorbent experienced minor changes in their locations compared to before adsorption. The detected peaks exhibited a shift in their respective wavenumbers, notably from 3,673 cm^{-1} to 3,651 cm^{-1}, 1,651 cm^{-1} to 1,652 cm^{-1}, 1,043 cm^{-1} to 1,000 cm^{-1}, and 782 cm^{-1} to 780 cm^{-1}. Therefore, the adsorption of BG can be attributed to the effectiveness of silanol (Si-OH) and siloxane (Si-O-Si) in adsorbing the dye. These assignments have the potential to demonstrate how dye molecules adhere to the surface of the adsorbent. This phenomenon occurred as a result of the interaction between positively charged dye sites and negatively charged deprotonated silanol sites [37]. Furthermore, the n-π interaction can occur between the lone pair electrons (n) located on oxygen, which are present in siloxane and silanol groups, and the π electrons situated on the aromatic rings of dye molecules [23].

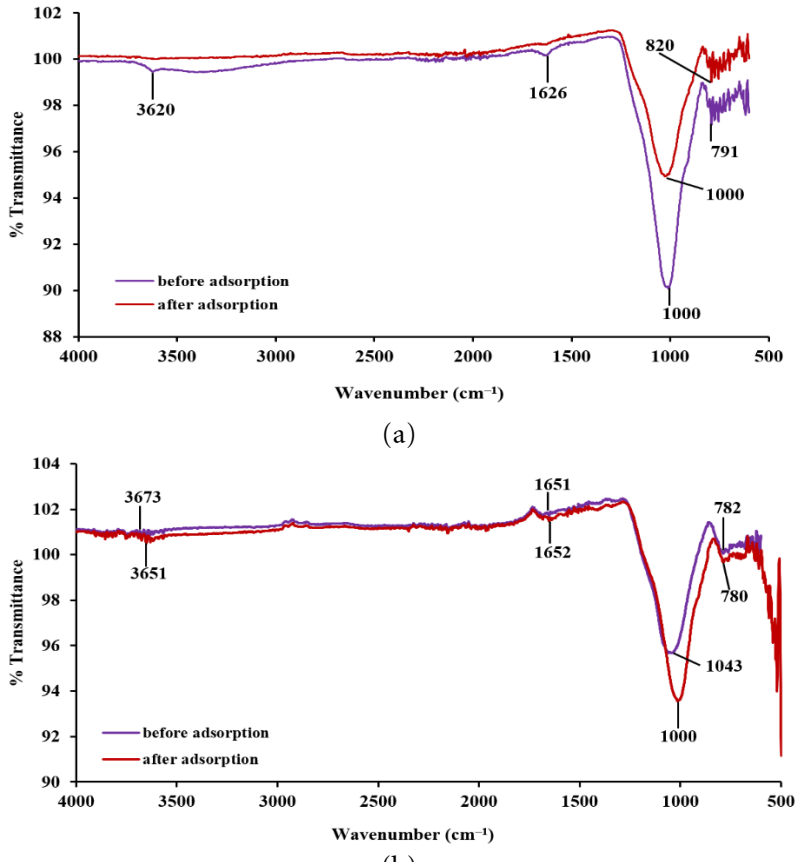

Figure 6 FT-IR spectrum before and after BG dye adsorption on the (a) raw and (b) modified pumice.

2) Adsorption study

2.1) Effect of pH

The pH level of the dye solution plays a crucial role in the process of adsorption. The pH influences the surface charge, the functional groups of the adsorbent, and the adsorbate structure [23]. When the pH of the solution exceeds the pH_{pzc} value (pH= 6.3 and 5.7 for the raw and modified pumice) the surface of the adsorbent acquires a negative charge. Nevertheless, in cases when the pH of the solution is below the pH_{pzc}, the surface of the adsorbent becomes positively charged. To investigate the effect of pH, batch adsorption experiments were performed using a BG dye solution at a concentration of 100 mg L^{-1}. The pH was varied from 2 to 10, with all other variables held constant. The outcomes of this investigation are illustrated in Figure 7. The adsorption

capacity showed a significant increase; raw pumice expanded from 6.44 to 16.91 mg g^{-1}, and modified pumice climbed from 6.85 to 19.06 mg g^{-1}, as the pH level rose from 2 to 8. Both adsorbents reached their peak adsorption capacity at a pH level of 8 or higher.

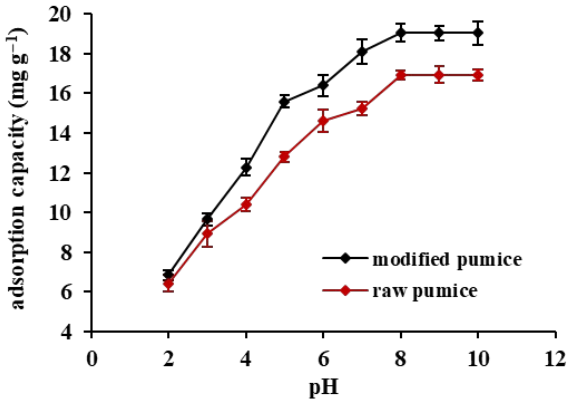

Figure 7 Influence of pH on adsorption (pH = 2-10; BG dye concentration 100 mg L^{-1}; contact time 180 min; raw and modified pumice dose 0.5 g; temperature 30°C).

When the pH of the BG^+ solution decreases below the pH_{pzc}, the silanol groups (Si-OH) present on the surface of the adsorbent acquire a positive charge, as illustrated in Eq. 16. The repulsive forces between BG^+ and the positively charged surface lead to an unsatisfactory adsorption outcome.

$$Si\text{-}OH + H^+ \rightarrow SiOH_2^+ \quad \text{(Eq. 16)}$$

When the pH of the BG^+ solution overcomes pH_{pzc}, the surface of the adsorbent (Si-OH) acquires a negative charge, as seen in Eq. 17. The considerable electrostatic attraction between the negatively charged adsorbent surface and the positively charged BG^+ dye molecules may account for its high adsorption capacity. Consequently, the adsorption of BG^+ is favored at a pH level that exceeds the pH at the pH_{pzc}. The process through which BG^+ dye is adsorbed can be shown by Eq. 18.

$$Si\text{-}OH + OH^- \rightarrow Si\text{-}O^- + H_2O \quad \text{(Eq. 17)}$$

$$Si\text{-}O^- + BG^+ \rightarrow Si\text{-}O^-\ BG^+ \quad \text{(Eq. 18)}$$

2.2) Effect of contact time and initial dye concentration

One of the adsorption parameters is the contact time between the adsorbate and the adsorbent. The adsorption capacity increases as the contact time increases, and then the adsorption becomes constant at equilibrium. To investigate the effects of contact time and initial dye concentration, a sequence of batch adsorption tests was performed. The experiments utilized a BG dye solution at concentrations of 50, 100, and 200 mg L^{-1}. All other variables remained constant. Data on adsorption were gathered at various contact times ranging from 5 to 300 minutes. The graphical representation depicted in Figure 8 illustrates the impact of contact time on different BG dye concentrations. The study's findings indicated that the adsorption capacity positively correlated with the time of contact, ultimately reaching a steady-state adsorption value after 180 minutes for all BG dye concentrations. The adsorption rate showed a significant initial increase during the first 15 minutes, then a subsequent decline until reaching a state of equilibrium. Over the time intervals of 5 to 180 minutes, the adsorption capacity increased from 3.71 to 7.95 mg g^{-1}, 7.59 to 15.98 mg g^{-1}, and 16.25 to 29.63 mg g^{-1} for the raw pumice, and from 3.61 to 9.54 mg g^{-1}, 9.60 to 19.05 mg g^{-1}, and 20.69 to 34.21 mg g^{-1} for the modified pumice, corresponding to dye concentrations of 50, 100, and 200 mg L^{-1}, respectively.

The fast adsorption seen during the early stage can be attributed to the ample presence of active sites on the surface, which carry a negative charge. Then, the adsorption became less efficient and approached equilibrium when these sites were gradually occupied [24].

The experimental results (Figure 8) showed that when the initial dye concentration was increased from 50 mg L^{-1} to 100 mg L^{-1} to 200 mg L^{-1}, respectively, there was an increase in the equilibrium adsorption capacity from 7.95 mg g^{-1} to 15.98 mg g^{-1} to 29.63 mg g^{-1} for the raw pumice and 9.54 mg g^{-1} to 19.05 mg g^{-1} to 34.21 mg g^{-1} for the modified pumice, respectively. The observed phenomena may be ascribed to the heightened driving force exerted by the concentration gradient for mass transfer, which exhibits a direct correlation with the initial concentration of the dye [38]. Adsorption of BG by modified clays [8] yielded similar findings.

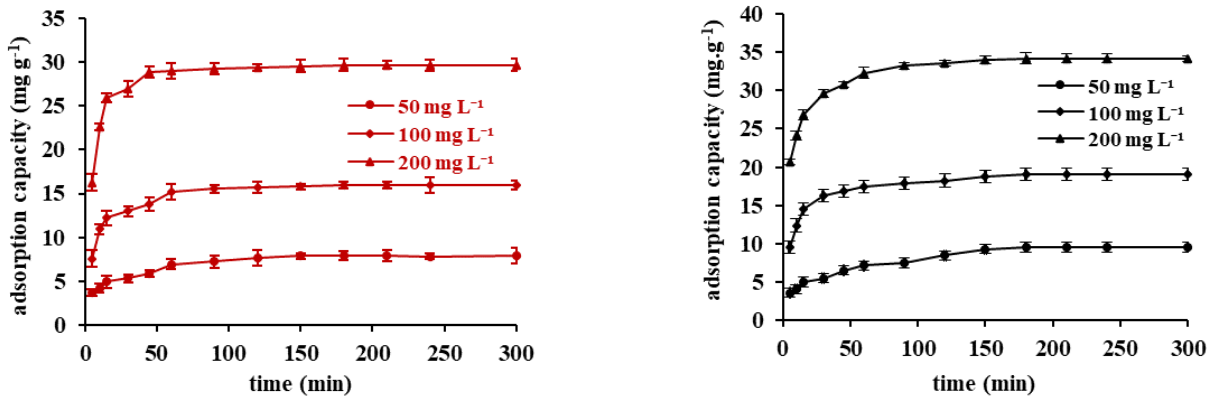

Figure 8 Influence of contact time and initial BG dye concentration on adsorption on (a) raw and (b) modified pumice (pH = 8; contact time 5-300 min; initial dye concentrations 50-200 mg L^{-1}; raw pumice and modified pumice dose 0.5 g; temperature 30°C).

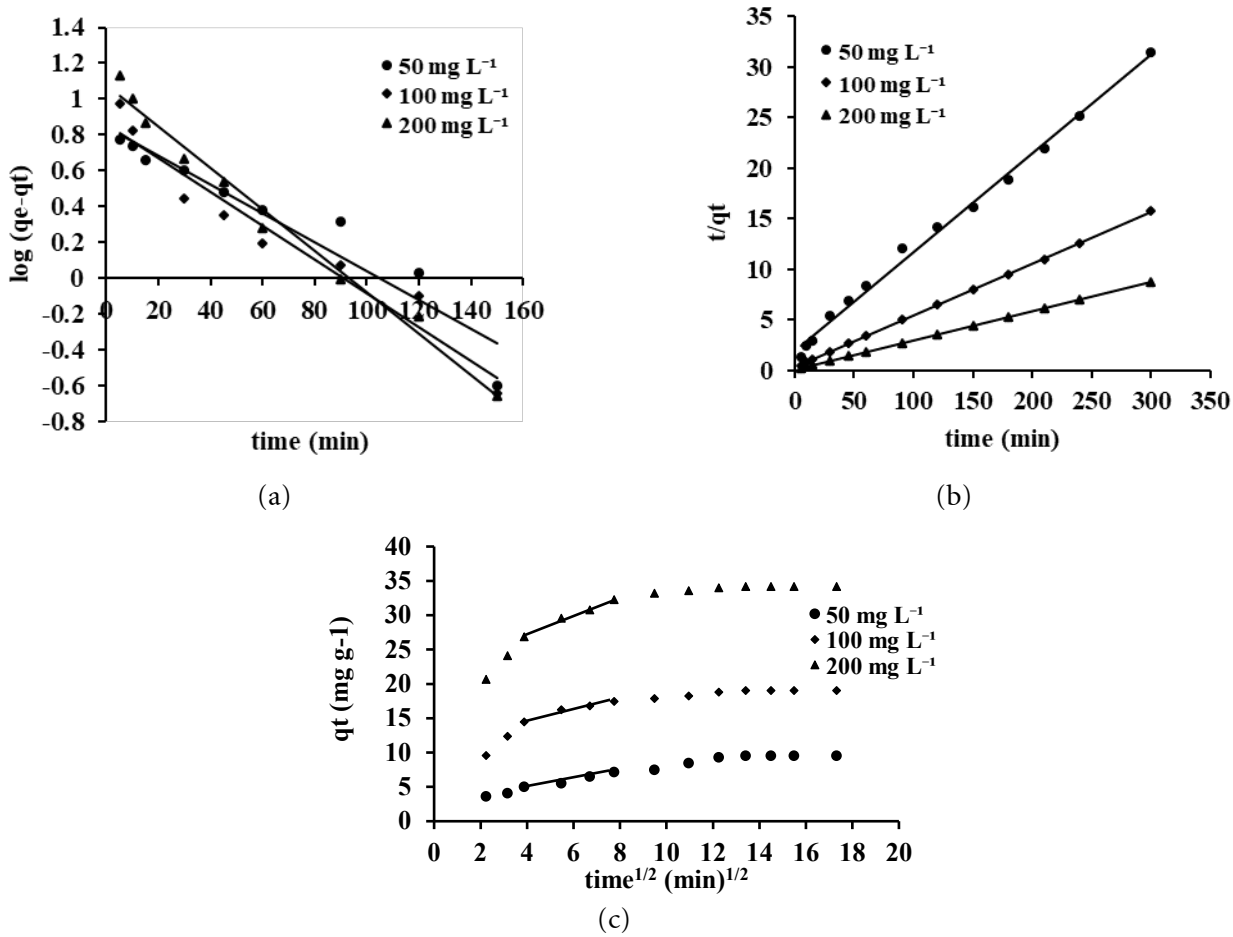

Figure 9 Adsorption kinetic of BG dye on the modified pumice (a) pseudo-first-order, (b) pseudo-second-order, and (c) intraparticle diffusion.

2.3) Adsorption kinetics

The research utilized three different kinetic models of adsorption—pseudo-first order, pseudo-second order, and intraparticle diffusion—to evaluate the adsorption data of both raw and modified pumice. Figure 9 presents only the kinetic adsorption models for the modified pumice and excludes those for the raw pumice. Meanwhile, Table 3 provides the calculated kinetic parameters for adsorption onto the raw and modified pumice. The R^2 value presented in Table 3 implies that the pseudo-second-order model more precisely represents the adsorption processes compared to the pseudo-first-order model and intraparticle diffusion. Furthermore, the adsorption capacity values obtained from the pseudo-second-order model are closer to the actual observed values. Therefore, the adsorption process involves the movement of liquids across the membrane, the attachment of substances to

the surface, and the internal movement of particles within the membrane, as detailed by Zhu et al. [23]. In addition, it was observed that a rise in concentrations led to a corresponding increase in the initial adsorption rate (h). In contrast, the rate constant of adsorption (k_2) exhibited a fairy constant [39]. The observed values of h demonstrated an upward trend in response to the elevated concentration levels, which may be attributed to the substantial influence of mass transfer as the driving factor.

The intraparticle diffusion model was utilized to analyze the kinetic adsorption findings to elucidate the diffusion mechanism. The plots displayed three distinct phases, as seen in Figure 9c. During the first phase, the molecules of BG exhibited rapid movement from the bulk solution toward the surface of the adsorbent, facilitated by a phenomenon known as boundary layer diffusion. This filled the pores on the surface of the adsorbent. The second stage, intraparticle diffusion, started at 15 to 180 minutes, and the third stage showed the attainment of the equilibrium stage. The absence of plots passing through the origin suggests that intra-particle diffusion was not the only thing that controlled the dye adsorption process. Determining the intercept value (C) provided insights into the thickness of the boundary layer in the adsorption process. The C's high values indicate the significant mass transfer of BG dye onto the raw and modified pumice material, indicating its importance in the sorption process [40]. This transfer predominantly occurs during the first adsorption stage. The data shown in Figure 9c and Table 3 indicate that the first linear segment of the curve corresponds to surface adsorption, whereas the second linear segment corresponds to the gradual transport of the adsorbate into the tiny holes of the adsorbent. Therefore, the adsorption of BG onto the modified pumice included both surface adsorption and intraparticle diffusion concurrently [41].

2.4) Adsorption isotherm and effect of temperature

Adsorption experiments were carried out at three different temperatures (20°C, 30°C, and 40°C) to establish the isotherm for dye adsorption. The experiments tested various concentrations, held constant at each temperature, to examine the impact of initial dye concentrations ranging from 50 to 300 mg L^{-1} at equilibrium time. Figure 10 (a and b) depicts the experimental outcomes demonstrating the correlation between the equilibrium concentration (C_e) and the adsorption capacity (q_e) for raw and modified pumice. The experimental findings indicated a direct correlation between the quantity of BG dye and the adsorption capacity of the raw and modified pumice. The adsorption capacity continued to rise until it reached a saturation point. The observed behavior may be explained by the increased driving force caused by the concentration gradient of mass transfer between the adsorbate in the aqueous phase and the solid phase of the adsorbent. A similar observation was the removal of crystal violet dye by diatomaceous earth [34].

Table 3 Adsorption kinetic parameters of BG dye by raw pumice and modified pumice

Kinetic models	Raw pumice			Modified pumice		
	BG dye concentration (mg L^{-1})			BG dye concentration (mg L^{-1})		
	50	100	200	50	100	200
q_e (mg g^{-1})	7.95	15.98	29.63	9.54	19.05	34.21
Pseudo-first order						
q_e (mg g^{-1})	5.43	6.18	6.81	6.99	7.20	8.45
k_1 (min^{-1})	0.027	0.026	0.029	0.019	0.022	0.026
R^2	0.967	0.945	0.899	0.918	0.945	0.955
Pseudo-second order						
q_e (mg g^{-1})	8.28	16.37	30.03	10.26	19.49	34.84
k_2 (g mg^{-1} min^{-1})	0.011	0.011	0.012	0.004	0.008	0.006
h (mg g^{-1} min^{-1})	0.754	2.948	10.822	0.421	3.039	7.770
R^2	0.999	0.999	0.999	0.995	0.999	0.999
Intraparticle diffusion						
K_{id} (mg g^{-1} $min^{-1/2}$)	0.495	0.744	0.870	0.569	0.758	1.369
C (mg g^{-1})	2.848	9.129	22.450	2.662	11.746	21.742
R^2	0.889	0.931	0.987	0.965	0.959	0.988

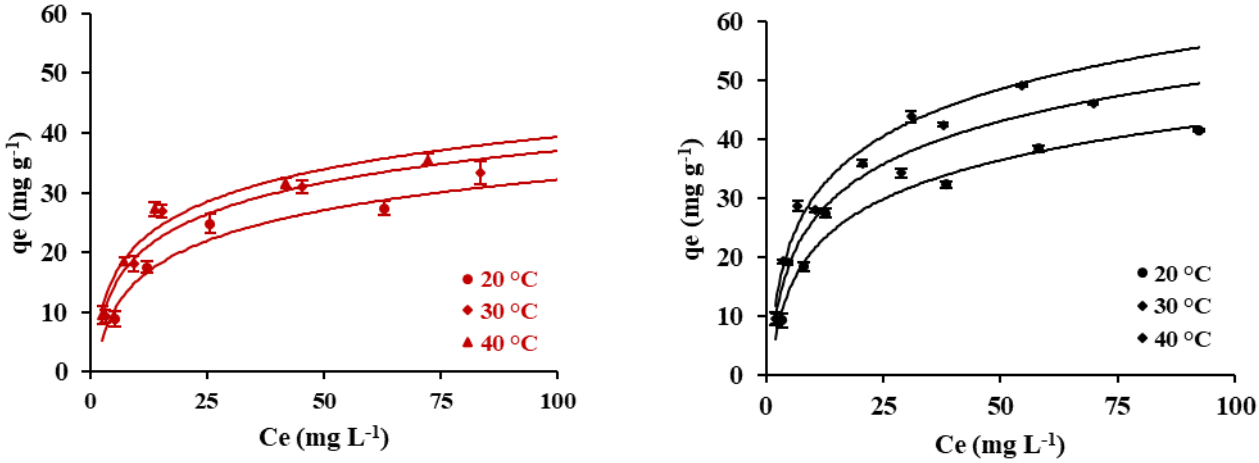

Figure 10 Isotherm of BG adsorption on the (a) raw and (b) modified pumice (initial BG concentrations 50, 100, 150, 200, 250, 300 mg L^{-1}, contact time 180 min, temperatures 20°, 30°, 40°C, raw pumice and modified pumice dose 0.5 g, pH 8).

In addition, Figure 10 shows a positive relationship between the adsorption capacity and the adsorption temperatures. This suggests that the adsorption process is endothermic. Jiang et al. [42] proposed that an increase in temperature facilitates enhanced particle mobility during adsorption. As a result, the possibility of adsorbate molecules coming into contact with the functional groups on the surface of the adsorbent was increased, hence boosting the adsorption capacity. In their study, Kurniawan et al. [37] discovered that the effectiveness of removing two cationic dyes, methylene blue and malachite green, was improved with increasing temperatures when utilizing bentonite and rarasaponin-bentonite as adsorbents.

The computed parameters for the linear Langmuir, Freundlich, and Dubinin-Radushkevich isotherm models of BG adsorption onto the raw and modified pumice are included in Table 4. The correlation coefficient (R^2) presented in Table 4 indicates a significant agreement between the experimental equilibrium data and the Langmuir isotherm, beyond the goodness of fit achieved by both the Freundlich and Dubinin-Radushkevich isotherms. Indications point to the presence of a monolayer that envelops the surface where the sorbed molecules are located. The adsorption capacity (q_{max}) reached its highest value at temperatures of 20°, 30°, and 40°C, with corresponding values of 37.13, 40.17, and 42.73 mg g^{-1} for the raw pumice and 46.72, 51.81, and 56.17 mg g^{-1} for the modified pumice, respectively. Modified pumice is superior in adsorption compared to raw pumice due to its electrically charged and hydrophilic surface. Raw pumice is not particularly effective at adsorbing hydro-phobic organic molecules from aqueous solutions. Moreover, treating natural adsorbent with acid can significantly enhance its ability to remove hydrophobic contaminants from water [43].

In addition, the observed values of the separation factor (R_L) were all below 1, indicating good adsorption of BG dye onto the raw and modified pumice [2]. R_L values were lower at higher concentrations and higher temperatures. This means that higher adsorption occurs at higher concentrations and higher temperatures.

The Freundlich isotherm showed favorable adsorption with 1/n values below 1, suggesting a typical Langmuir isotherm [41]. At higher adsorption temperatures, the rise in K_F indicates an increase in the number of active sites, whereas the increase in 1/n can be interpreted as a greater degree of surface heterogeneity in the adsorption process. The physical adsorption of BG dye is indicated by the mean free energy (E) values from the Dubinin-Radushkevich isotherm, which are 0.378, 0.577, and 0.707 kJ mol^{-1} for the raw pumice, and 0.577, 0.707, and 1.000 kJ mol^{-1} for the modified pumice at temperatures of 20°, 30°, and 40°C, respectively [22].

2.5) Thermodynamic study and removal efficiency

The thermodynamic experiments were performed to investigate the adsorption behavior of BG dye onto the raw and modified pumice at three distinct temperatures: 20°, 30°, and 40°C. It was ensured that the system reached a state of equilibrium during the testing. The adsorption data were utilized to calculate the equilibrium constants ($K_e = q_e/C_e$), which were subsequently transformed into ΔG using Eq. 12. Furthermore, the values of ΔH and ΔS were obtained by analyzing the slope and intercept of the graph depicting the logarithm K_e against the reciprocal of temperature (1/T), as seen in Figure 11(a).

Table 4 Isotherm parameters of BG by the raw pumice and modified pumice

Isotherm	Raw pumice			Modified pumice		
	Temperature (°C)			Temperature (°C)		
	20	30	40	20	30	40
Langmuir isotherm						
q_{max} (mg g^{-1})	37.13	40.17	42.73	46.72	51.81	56.17
K_L (L mg^{-1})	0.06	0.09	0.10	0.07	0.10	0.11
R_L	0.247-0.052	0.182-0.036	0.163-0.031	0.222-0.045	0.167-0.032	0.154-0.029
R^2	0.978	0.991	0.095	0.994	0.990	0.991
Freundlich isotherm						
K_F (mg g^{-1})/(mg $L^{-1})^{1/n}$	5.91	7.51	8.28	7.04	8.38	9.26
1/n	0.38	0.36	0.36	0.41	0.43	0.45
R^2	0.895	0.888	0.907	0.895	0.924	0.896
Dubinin-Radushkevich isotherm						
q (mg g^{-1})	2.219	2.612	2.813	33.49	36.39	39.62
E (kJ mol^{-1})	0.378	0.577	0.707	0.577	0.707	1.000
R^2	0.908	0.870	0.867	0.855	0.894	0.931

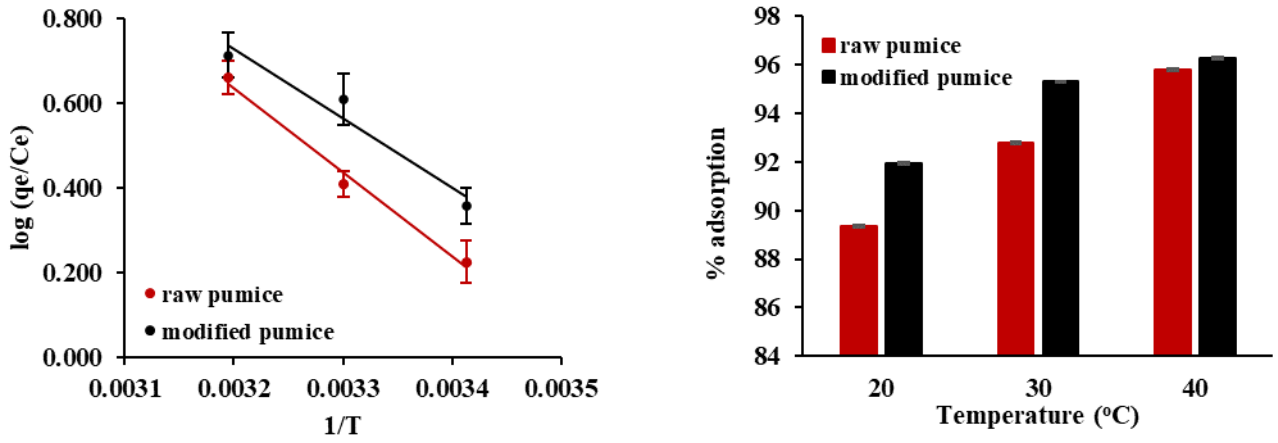

(a) (b)

Figure 11 (a) Thermodynamics and (b) removal efficiency (%) of BG adsorption onto the raw and modified pumice. (pH = 8; BG dye concentration 100 mg L-1; contact time 180 min; raw and modified pumice dose 0.5 g; temperature 20°- 40 C).

The adsorption studies indicated that at 20°, 30°, and 40°C, the ΔG values for raw pumice were -0.09, -0.23, and -0.51 kJ mol^{-1}, respectively, while for modified pumice, the values were -0.13, -0.34, and -0.54 kJ mol^{-1}. As the temperature increased, the values of ΔG became increasingly negative. The spontaneous and favorable adsorption of the BG dye can be attributed to the negative values of ΔG. Therefore, the adsorption was more favorable at higher temperatures. The determined value for ΔH was found to be 32.12 kJ mol^{-1} for raw pumice and 34.00 kJ mol^{-1} for modified pumice, while the estimated value for ΔS was determined to be 0.13 J mol^{-1} for raw pumice and 122.92 J mol^{-1} for modified pumice, respectively. The adsorption process exhibited an endothermic nature due to the positive value of ΔH. Also, Al-Shehri et al. [2] showed that the adsorption of crystal violet onto Aerva javanica leaves was physisorption when the ΔH value was between 20 and 40 kJ mol^{-1}. Hence, the adsorption of BG onto the raw and modified pumice may be ascribed to physisorption, which serves as the primary mechanism. Since the value of ΔS was determined to be positive, it may be deduced that the adsorption process increased entropy. The observed phenomena can be ascribed to an increased degree of randomness at the interface of the solid-solution system during the adsorption process. Duran et al. [4] observed comparable thermodynamic results in their study on the adsorption of three basic dyes onto almond shells (*Prunus dulcis*).

The experimental data on adsorption, collected at three different temperatures, demonstrated that the removal efficiency, depicted in Figure 11(b), was determined using Eq. 3. The findings presented in Figure 11(b) suggest that the removal efficiency increased with

a temperature rise. Additionally, the BG removal efficiency was invariably greater with modified pumice (91.93%, 95.29%, 96.27%) compared to raw pumice (89.34%, 92.76%, 95.80%) at the respective temperatures of 20°, 30°, and 40°C.

2.6) Mechanism of BG adsorption on modified pumice

To understand the adsorption mechanism, it is essential to consider both the adsorbate's structural characteristics and the adsorbent's surface qualities. The substance being adsorbed is a BG dye, specifically classified as a cationic dye. The study focused on the adsorption mechanism created by the modified pumice, primarily composed of Si-OH and Si-O-Si groups. Pumice can generate a negative charge at pH levels higher than its pH_{pzc}. The adsorption mechanism of BG dye onto the modified pumice, as seen in Figure 12, may be ascribed to various interactions. These interactions include dipole-dipole H-bonding, Yoshida H-bonding, electrostatic interaction, n-π interaction, pore filling, and cation exchange. The FTIR analysis indicated changes on the surface of the modified pumice material due to adsorption. The adsorption of BG caused a change in the maxima of the hydroxyl groups, moving them from 3,673 cm^{-1} to 3,651 cm^{-1} and 1,651 cm^{-1} to 1,652 cm^{-1}. These findings indicate that dipole-dipole H-bonding interactions and Yoshida H-bonding influence adsorption. An interaction occurred between the nitrogen atom in the BG dye and the hydrogen atom connected to oxygen (OH) on the surface of the adsorbent, involving dipole-dipole hydrogen bonds. The hydrogen atom in the hydroxyl group (OH) on the adsorbent surface interacts with the π electrons located within the aromatic ring of the dye, resulting in the establishment of Yoshida H-bonding. Furthermore, the FTIR peaks corresponding to the siloxane and silanol groups shifted from 1,043 cm^{-1} to 1,007 cm^{-1} and from 782 cm^{-1} to 780 cm^{-1}, indicating the involvement of n-π interaction in the adsorption process. The n-π interaction arose from the interaction between the π electrons derived from the aromatic rings of the dye and the lone pair electrons (n) of an oxygen atom on the adsorbent's surface.

Adsorption occurs when the pH is higher than the pHpzc, resulting in an electrostatic contact between the positively charged component (N^+) of the dye and the negatively charged component ($Si\text{-}O^-$) on the surface of the modified pumice, which is made up of silica groups. Regarding the kinetic study, BG demonstrated fast migration from the main solution to the surface of the modified pumice and thereafter filled the pores. Moreover, the adsorbent possesses a coarse surface with uneven grooves that have been empirically proven to enhance the process of pore-filling during adsorption. A significant reduction in the concentration of some components, specifically K_2O and Fe_2O_3, was detected throughout the adsorption process. This discovery implies that they may be participating in the cation exchange process between the BG^+ dye molecules and certain elements found on the surfaces of the modified pumice.

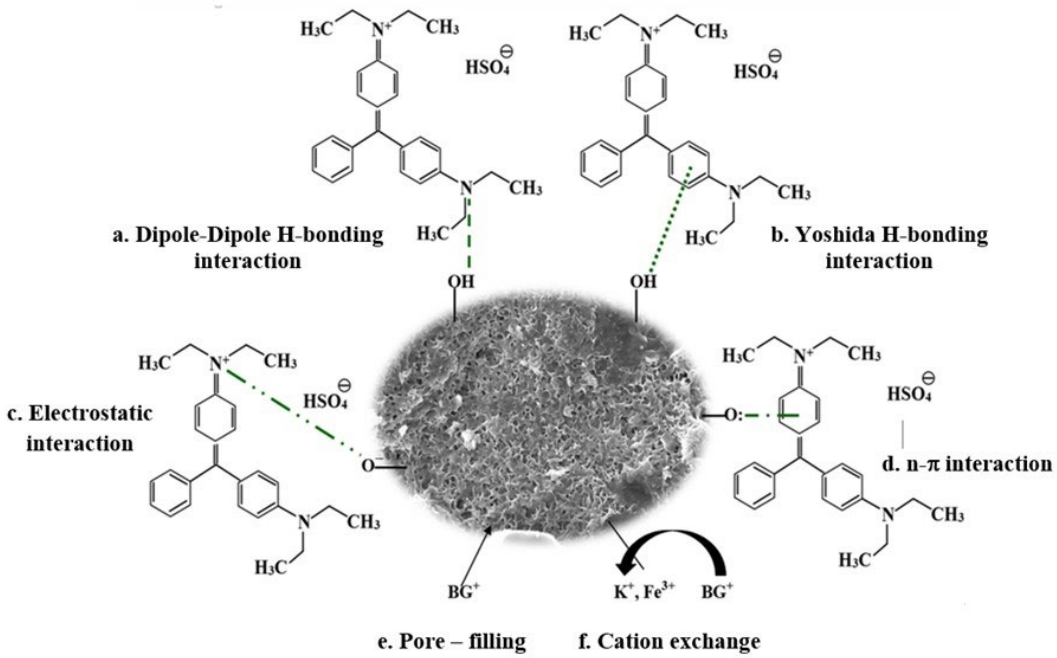

Figure 12 BG adsorption mechanism.

Conclusion

The primary objective of this investigation was to examine the process of adsorption and the deeper mechanisms involved in the adsorption of BG dye onto the modified pumice adsorbent. This study characterized the raw and modified pumice using nitrogen adsorption-desorption isotherms, XRD, XRF, FTIR, SEM, and pH_{pzc}. The studies indicated that both raw and modified pumice samples possess mesoporous structures. The BET surface area measurements were 12.020 ml g^{-1} for the raw pumice and 3.739 ml g^{-1} for the modified pumice. The primary active groups on the surface of the raw and modified pumice contained functional groups like silanol (Si-OH) and siloxane (Si-O-Si). The experimental investigation involved studying the adsorption behavior of BG dye onto raw pumice and HCl-treated pumice. The adsorption procedure took into account several factors, including pH (2–10), contact time (5–300 min), dye concentrations (50–300 mg L^{-1}), and temperatures (20°–40°C). The experimental results revealed that the most favorable conditions for the process were achieved at a pH value of 8 and a contact time of 180 minutes for both adsorbents. The Langmuir isotherm provided the most accurate fit for the equilibrium adsorption data, with maximum adsorption capacities of 37.13, 40.17, and 42.73 mg g^{-1} for the raw pumice and 46.72, 51.81, and 56.17 mg g^{-1} for the modified pumice at temperatures of 20°, 30°, and 40°C, respectively. The BG adsorption process was consistent with the pseudo-second-order model for both adsorbents. The thermodynamic investigation demonstrated that the process of BG adsorption took place spontaneously, and it was determined to be a form of physisorption. The adsorption mechanism of BG dye on the modified pumice involved many interactions such as dipole-dipole hydrogen bonding, Yoshida hydrogen bonding, electrostatic interaction, n-$\boldsymbol{\pi}$ interaction, pore filling, and cation exchange. The modified pumice showed a higher efficiency percentage in removing BG dye than its raw counterpart. In summary, the HCl-treated pumice has been successfully utilized as an efficient and reliable adsorbent to remove BG dye from an aqueous solution.

References

[1] Gurses, A., Gune , K., Sahin, E., Acikyildiz, M. Investigation of the removal kinetics, thermodynamics and adsorption mechanism of anionic textile dye, Remazol Red RB, with powder pumice, a sustainable adsorbent from wastewater. Frontiers in Chemistry, 2023, 11, 1156577.

[2] Al-Shehri, H.S., Almudaifer, E., Alorabi, A.Q., Alanazi, H.S., Alkorbi, A.S. Effective adsorption of crystal violet from aqueous solutions with effective adsorbent: equilibrium, mechanism studies and modeling analysis. Environmental Pollutants and Bioavailability, 2021, 33(1), 214–226.

[3] Patawat, C., Silakate, K., Chuan-Udom, S., Supanchaiyamat, N., Hunt, A.J., Ngernyen, Y. Preparation of activated carbon from Dipterocarpus alatus fruit and its application for methylene blue adsorption. RSC Advances, 2020, 10(36), 21082–21091.

[4] Duran, C., Ozdes, D., Gundogdu, A., Senturk, H.B. Kinetics and isotherm analysis of basic dyes adsorption onto almond shell (Prunus dulcis) as a low-cost adsorbent. Journal of Chemical & Engineering Data, 2011, 56(5), 2136–2147.

[5] Rehman, R., Muhammad, S.J., Arshad, M. Brilliant green and acid orange 74 dyes removal from water by Pinus roxburghii leaves in naturally benign way: An application of green chemistry. Journal of Chemistry, 2019, 3573704.

[6] El-Sayed, E.M., Hamad, H.A., Ali, R.M. Journey from ceramic waste to highly efficient toxic dye adsorption from aqueous solutions via one-pot synthesis of CaSO4 rod-shape with silica. Journal of Materials Research and Technology, 2020, 9(6), 16051–16063.

[7] Ullah, S., Ur Rahman, A., Ullah, F., Rashid, A., Arshad, T., Viglasova, E., Ullah, H. Adsorption of malachite green dye onto mesoporous natural inorganic clays: Their equilibrium isotherm and kinetics studies. Water, 2021, 13(7), 965.

[8] Ullah, R., Iftikhar, F.J., Ajmal, M., Shah, A., Akhter, M.S., Ullah, H., Waseem, A. Modified clays as an efficient adsorbent for brilliant green, ethyl violet and allura red dyes: Kinetic and thermodynamic studies. Polish Journal of Environmental Studies, 2020, 29(5), 3831–3839.

[9] Uner, O., Gecgel, U., Bayrak, Y. Adsorption of methylene blue by an efficient activated carbon prepared from Citrullus lanatus Rind: Kinetic, isotherm, thermodynamic, and mechanism analysis. Water, Air, & Soil Pollution, 2016, 227, 247.

[10] Nirmaladevi, S., Palanisamy, N. A comparative study of the removal of cationic and anionic dyes from aqueous solutions using biochar as an adsorbent. Desalination and Water Treatment, 2020, 175, 282–292.

[11] Sogut, E.G., Ergana, E., Kilicb, N.C., Donmezb, H., Akba b, E. Methylene blue adsorption from aqueous solution by functionalized perlites: An experimental and computational chemistry study. Desalination and Water Treatment, 2021, 217, 391–410.

[12] Mourhly, A., Khachani, M., Hamidi, A.E., Kacimi, M., Halim, M., Arsalane, S. The synthesis and characterization of low-cost mesoporous silica SiO_2 from local pumice rock. Nanomaterials and Nanotechnology, 2015, 5, 35.

[13] Biswas, B., Islam, M.R., Deb, A.K., Greenaway, A., Warr, L.N, Naidu, R. Understanding iron impurities in Australian kaolin and their effect on acid and heat activation processes of clay. ACS Omega, 2023, 8, 5533–5544.

[14] Olasehinde, E.F., Abegunde, S.M. Adsorption of methylene blue onto acid modified Raphia Taedigera seed activated carbon. Advanced Journal of Chemistry, 2020, A3(5), 663–679.

[15] Indah, S., Helard, D., Primasari, B., Edwin, T., Andeslin, S, Performance evaluation of physically and chemically modified pumice on removal of Cu(II) from aqueous solution. Trends in Science, 2022, 19(4), 2585.

[16] Silva, V.C., Araujo, M.E.B., Rodrigues, A.M., Cartaxo, J.M., Menezes, R.R., Neves, G.A. Adsorption behavior of acid—treated Brazillian Palygorskite for cationic and anionic dyes removal from the water. Sustainability, 2021, 13, 3954.

[17] Akbal, F. Adsorption of basic dyes from aqueous solution onto pumice powder. Journal of Colloid and Interface Science, 2005, 286(2), 455–458.

[18] Samarghandi, M.R., Zarrabi, M., Sepehr, M.N., Amrane, A., Safari, G.H., Bashiri, S. Application of acidic treated pumice as an adsorbent for the removal of azo dye from aqueous solutions: kinetic, equilibrium and thermodynamic studies. Iranian Journal of Environmental Health, Science and Engineering, 2012, 9, 1–10.

[19] Shayesteh, H., Rahbar-Kelishami, A., Norouzbeigi, R. Adsorption of malachite green and crystal violet cationic dyes from aqueous solution using pumice stone as a low-cost adsorbent: Kinetic, equilibrium, and thermodynamic studies. Desalination and Water Treatment, 2016, 57(27), 12822–12831.

[20] Yavuz, M., Gode, F., Pehlivan, E., Ozmert, S., Sharma, Y.C. An economic removal of Cu^{2+} and Cr^{3+} on the new adsorbents: Pumice and polyacrylonitrile/pumice composite. Chemical Engineering Journal, 2008, 137(3), 453–461.

[21] Soleimani, H., Sharafi, K., Parian, J.A., Jaafari, J., Ebrahimzadeh, G. Acidic modification of natural stone for Remazol Black B dye adsorption from aqueous solution-central composite design (CCD) and response surface methodology (RSM). Heliyon, 2023, 9, e14743.

[22] Dinh, V-P., Huynh, T-D-T., Le, H.M., Nguyen, V-D., Dao, V.A., Hung, N.Q., …, Tan, L.V. Insight into the adsorption mechanisms of methylene blue and chromium (III) from aqueous solution onto pomelo fruit peel. RSC Advances, 2019, 9(44), 25847–25860.

[23] Zhu, Y., Yi, B., Yuan, Q., Wu, Y., Wang, M., Yan, S. Removal of methylene blue from aqueous solution by cattle manure-derived low temperature biochar. RSC Advances, 2018, 8(36), 19917–19929.

[24] Sun, Y., Li, Y., Chen, B., Wang, M., Zhang, Y., Chen, K., …, Pi, X. Methylene blue removed from aqueous solution by encapsulation of bentonite aerogel beads with cobalt alginate. ACS Omega, 2022, 7, 41246–41255.

[25] Seifi, S., Levacher, D., Razakamanantsoa, A., Sebaibi, N. Microstructure of dry mortars without cement: Specific surface area, pore size and volume distribution analysis. Applied Sciences, 2023, 13, 5616.

[26] Ikhtiyarova, G.A., Ozcan, A.S., Gok, O., Ozcan, A. Characterization of natural- and organo bentonite by XRD, SEM, FT-IR and thermal analysis techniques and its adsorption behaviour in aqueous solutions. Clay Minerals, 2012, 47(1), 31–44.

[27] Alexander, J.A., Zaini, M.A.A., Abdulsalam, S., El-Nafaty, U.A., Aroke, U.O. Physicochemical characteristics of surface modified Dijah-Monkin bentonite. Particulate Science and Technology, 2018, 36(3), 1245689.

[28] Zhang, H., Zhou, J., Muhammad, Y., Tang, R., Liu, K., Zhu, Y., Tong, Z. Citric acid modified bentonite for Congo Red adsorption. Frontiers in Materials, 2019, 6(5), 1–11.

[29] Mansour, R., Simeda, M.G., Zaatout, A. Adsorption studies on brilliant green dye in aqueous solutions using activated carbon derived from guava seeds bb chemical activation with phosphoric acid. Desalination and Water Treatment, 2020, 202, 396–409.

[30] Biswas, S., Mishra, U. Effective Remediation of Lead ions from aqueous solution by chemically carbonized rubber wood sawdust: Equilibrium, kinetics, and thermodynamic study. Journal of Chemistry, 2015, 842707.

[31] Ersoy, B., Sariisik, A., Dikmen, S., Sariisik, G. Characterization of acidic pumice and determination of its electrokinetic properties in water. Powder Technology, 2010, 197, 129–135.

[32] Jedynak, K., Charmas, B. Preparation and characterization of physicochemical properties

of spruce cone biochars activated by CO_2. Materials, 2021, 14, 3859.

[33] De Castro, M.L.F.A., Abad, M.L.B., Sumalinog, D.A.G., Abarca, R.R.M., Paoprasert, P., de Luna, M.D.G. Adsorption of methylene blue dye and Cu(II) ions on EDTA-modified bentonite: Isotherm, kinetic and thermodynamic studies. Sustainable Environment Research, 2018, 28(5), 197–205.

[34] Castellar-Ortega, G.C., Cely-Bautistab, M.M., Cardozo-Arrieta, B.M., Jaramillo-Colpas, J.E., Jaramillo-Colpasc, L.C., Valencia-Rios, J.S. Evaluation of diatomaceous earth in the removal of crystal violet dye in solution. Journal of Applied Research and Technology, 2022, 20, 387–398.

[35] Dehghani, M.H., Hassani, A.H., Karri, R.R., Younesi, B., Shayeghi, M., Salari, M., …, Heidarinejad, Z. Process optimization and enhancement of pesticide adsorption by porous adsorbents by regression analysis and parametric modelling. Scientific Reports, 2021, 11, 11719.

[36] Sepehr, M.N., Amrane, A., Karimaian, K.A., Zarrabi, M., Ghaffari, H.R. Potential of waste pumice and surface modified for hexavalent chromium removal: Characterization, equilibrium, thermodynamic and kinetic study. Journal of the Taiwan Institute of Chemical Engineers, 2014, 45, 635–647.

[37] Kurniawan, A., Sutiono, H., Indraswati, N., Ismadji, S. Removal of basic dyes in binary system by adsorption using rarasaponin–bentonite: Revisited of extended Langmuir model. Chemical Engineering Journal, 2012, 189-190, 264–274.

[38] Popoola, L.T., Aderibigbe, T.Ad., Yusuff, A.S., Munir, M.M. Brilliant green dye adsorption onto composite snail shell-rice husk: Adsorption isotherm, kinetic, mechanistic and thermodynamics analysis. Environmental Quality Management, 2018, 28(2), 63–78.

[39] Doke, K.M., Khan, E.M. Equilibrium, kinetic and diffusion mechanism of Cr (VI) adsorption onto activated carbon derived from wood apple shell. Arabian Journal of Chemistry, 2017, 10, S252–S260.

[40] Maruthapandi, M., Kumar, V.B., Luong, J.H.T., Gedanken, A. Kinetics, Isotherm, and thermodynamic studies of methylene blue adsorption on polyaniline and polypyrrole–macro nanoparticles synthesized by C Dot-Initiated polymerization. ACS omega, 2018, 3(7), 7196–7203.

[41] Ciobanu, G., Barna, S., Harja, M. Kinetic and equilibrium studies on adsorption of Reactive Blue 19 dye from aqueous solutions by nanohydroxyapatite adsorbent. Archives of Environmental Protection, 2016, 42(2), 3–11.

[42] Jiang, L., Yu, H., Pei, L., Hou, X. The effect of temperature on the synergistic effect between a magnetic field and functionalized graphene oxide-carbon nanotube composite for Pb^{2+} and phenol adsorption. Journal of Nanomaterials, 2018, 9167938.

[43] Ullah, Z., Hussain, S., Gul, S., Khan, S., Bangash, F.K. Use of HCl-modified bentonite clay for the adsorption of Acid Blue 129 from aqueous solutions. Desalination and Water Treatment, 2015, 1027282.